

Green formulation for studying electromagnetic scattering from graphene-coated wires of arbitrary section

CLAUDIO VALENCIA,¹ MÁXIMO A. RISO,² MAURO CUEVAS,^{3,4} AND RICARDO A. DEPINE^{2,*}

¹Facultad de Ciencias, Universidad Autónoma de Baja California (UABC), Ensenada, BC 22860, Mexico

²Grupo de Electromagnetismo Aplicado, Departamento de Física, FCEN, Universidad de Buenos Aires and IFIBA, Consejo Nacional de Investigaciones Científicas y Técnicas (CONICET), Ciudad Universitaria, Pabellón I, C1428EHA, Buenos Aires, Argentina

³Facultad de Ingeniería y Tecnología Informática, Universidad de Belgrano, Villanueva 1324, C1426BMJ, Buenos Aires, Argentina

⁴Consejo Nacional de Investigaciones Científicas y Técnicas (CONICET), Av. Rivadavia 1917, C1033AAJ, Buenos Aires, Argentina

*Corresponding author: rdep@df.uba.ar

Received 5 December 2016; accepted 20 February 2017; posted 28 March 2017 (Doc. ID 282163); published 5 May 2017

We present a rigorous electromagnetic method based on Green's second identity for studying the plasmonic response of graphene-coated wires of arbitrary shape. The wire is illuminated perpendicular to its axis by a monochromatic electromagnetic wave and the wire substrate is homogeneous and isotropic. The field is expressed everywhere in terms of two unknown source functions evaluated on the graphene coating which can be obtained from the numerical solution of a coupled pair of inhomogeneous integral equations. To assess the validity of the Green formulation, the scattering and absorption efficiencies obtained numerically in the particular case of circular wires are compared with those obtained from the multipolar Mie theory. An excellent agreement is observed in this particular case, for both metallic and dielectric substrates. To explore the effects that the break of the rotational symmetry of the wire section introduces in the plasmonic features of the scattering and absorption response, the Green formulation is applied to the case of graphene-coated wires of elliptical section. As might be expected from symmetry arguments, we find a two-dimensional anisotropy in the angular optical response of the wire, particularly evident in the frequency splitting of multipolar plasmonic resonances. The comparison between the spectral position of the enhancements in the scattering and absorption efficiency spectra for low-eccentricity elliptical and circular wires allows us to guess the multipolar order of each plasmonic resonance. We present calculations of the near-field distribution for different frequencies which explicitly reveal the multipolar order of the plasmonic resonances. They also confirm the previous guess and serve as a further test on the validity of the Green formulation. © 2017 Optical Society of America

OCIS codes: (160.0160) Materials; (160.4760) Optical properties; (250.5403) Plasmonics; (290.0290) Scattering.

<https://doi.org/10.1364/JOSAB.34.001075>

1. INTRODUCTION

Due to its particular electronic band structure, the atom-thick form of carbon known as graphene exhibits unique electronic and optical properties that have attracted tremendous attention in recent years [1]. Several applications from terahertz (THz) to visible frequencies, including solar cells, touch screens, photo-detectors, light-emitting devices and ultrafast lasers, are clear evidence of the rise of graphene in photonics and optoelectronics [2,3]. The strength of the mutual interaction between graphene and electromagnetic radiation plays a key role in a great majority of these applications. However, a single sheet of homogeneous graphene exhibits an optical absorbance of $\sim 2.3\%$ [4], a value strong enough to detect exfoliated monolayers by visual inspection under an optical microscope but not sufficiently

strong as could be desirable in many photonics and optoelectronics applications.

The interaction between graphene and electromagnetic radiation can be improved in the presence of surface plasmons, whether by combining a graphene layer with conventional plasmonic nanostructures based on noble metals [5,6] or by taking advantage of the long-lived, electrically tunable surface plasmons supported by graphene [7,8]. The first alternative fits well in the visible and near-infrared frequencies where the interband loss becomes large and graphene behaves as a dielectric material, whereas the second alternative fits well in the terahertz and infrared regions where doped graphene nanostructures can support surface plasmons [7,8].

Surface plasmons can be roughly divided into two categories: surface plasmon polaritons propagating along waveguiding

structures and localized surface plasmons (LSPs) supported by spatially limited structures, such as scattering particles. Since the spatial periodicity associated with a surface plasmon propagating along a graphene monolayer is always less than the spatial periodicity which could be induced by an incident plane wave, plane waves cannot resonantly excite propagating surface plasmons at a flat graphene monolayer. In contrast, in bounded geometries, LSPs can be resonantly excited by plane waves at discrete frequencies that depend on the size and shape of the object to which they are confined.

The plasmonic properties of graphene-wrapped particles have recently attracted the attention of researchers [9–18]. Analytical solutions are only available for particles with a very simple shape, such as spheres [9–11] or circular cylinders [13–18]. In these cases, the application of Mie theory leads to multipole coefficients for the scattered field which have essentially the same form as those corresponding to the bare particles, except for additive corrections proportional to the graphene surface conductivity in the numerator and denominator. Taking into account the significant progress made in the fabrication of particles with a variety of shapes and dimensions [19] and that wrapping up particles with graphene coatings brings extra freedom for scattering engineering and for improving the interaction between graphene and electromagnetic radiation via surface plasmon mechanisms, the investigation of the scattering characteristics of graphene-coated particles seems a particularly interesting and very promising area to explore. In the particular case of dielectric, almost transparent particles, graphene coatings introduce tunable plasmons which are absent in the bare particle, whereas for metallic or metallic-like particles, graphene coatings can modify in a controlled manner the LSPs already existing in the bare particle.

The particular relation between the shape of a graphene particle and its plasmonic characteristics—such as cross-section enhancement, interplay between near- and far-field quantities, plasmon resonance frequencies, and linewidths—can be exploited in many terahertz applications, including the sensing of small changes in a host-medium refractive index caused by the change in concentration of an analyzed substance [18] or the design of subwavelength metamaterials [20]. In order to realize graphene-wrapped plasmonic particles with tailored properties for specific applications, complete electromagnetic solutions are needed. The purpose of this paper is to present a rigorous, fully retarded method based on Green's second identity [21–23] for modeling the scattering characteristics of graphene-coated, homogeneous dielectric or metallic two-dimensional particles (wires) of rather arbitrary shape.

The paper is organized as follows. First, in Section 2 we give exact expressions for the electromagnetic field scattered by a graphene-coated wire illuminated perpendicular to its axis by a p - or s -polarized monochromatic plane wave. The scattered field is expressed in terms of two unknown source functions evaluated on the wire surface, one related to the total field in the medium of incidence and the other related to its normal derivative. To find both surface source functions, a coupled pair of inhomogeneous integral equations must be solved numerically. In Section 3 the numerical technique is illustrated and validated for wires of circular and elliptical section. As a first

validation we consider metallic and dielectric circular wires and show that in this case the numerical results agree perfectly well with those obtained analytically using Mie's theory [15–17]. To explore the effects that the departure from circular geometries has on the scattering and extinction cross sections we then consider graphene-coated wires of elliptical section. We present scattering and absorption efficiency spectra showing that, similarly to the plasmonic resonances of bare metallic wires, the break of the rotational symmetry of the wire section introduces a two-dimensional anisotropy in the angular optical response of the wire, particularly evident in a frequency splitting of the strong dipolar plasmonic resonance [24,25], but also observable for higher multipolar resonances. Using the Green formulation, we show near-field distributions which reveal that the splittings correspond to strong localization of the near field at specific positions along the ellipse axes. In addition, and as a further test on the validity of the Green formulation, we show that the multipolar order inferred for ellipses with low eccentricities from the topology of the near-field distribution for a given resonant frequency is in excellent agreement with the multipolar order inferred from the spectral proximity between the enhancement peaks in the scattering efficiency spectra of an elliptical and a similar circular wire. Finally, in Section 4 we summarize and discuss the results obtained. The Gaussian system of units is used and an $\exp(-i\omega t)$ time dependence is implicit throughout the paper, with ω the angular frequency, c the speed of light in vacuum, t the time, and $i = \sqrt{-1}$.

2. GREEN'S APPROACH

We consider a wire in the form of an infinite cylinder whose axis lie along the \hat{z} -axis and whose cross section is defined by the planar curve Γ described by the vector valued function $\mathbf{r}_s(\tau) = f(\tau)\hat{x} + g(\tau)\hat{y}$ (see Fig. 1). The parameter τ can represent the arc length along the curve or any other convenient parameter, such as the angle θ . The wire substrate (region 2) is characterized by the electric permittivity ϵ_2 and the magnetic permeability μ_2 and is embedded in a transparent medium (region 1) with electric permittivity ϵ_1 and magnetic permeability μ_1 . This wire is coated with a graphene monolayer which can be considered as an infinitesimally thin, local, and isotropic two-sided layer with frequency-dependent surface conductivity

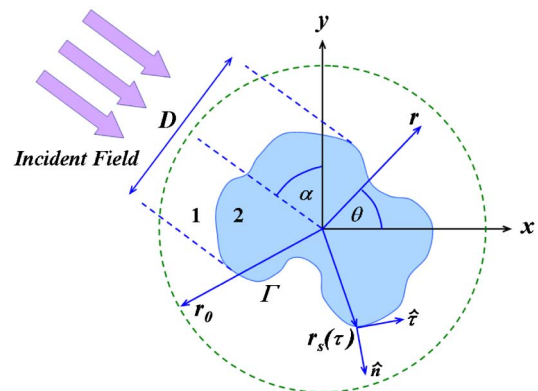


Fig. 1. Scattering configuration. The main section of the graphene-coated cylinder is defined by the planar curve Γ .

$\sigma(\omega) = \sigma^{\text{intra}} + \sigma^{\text{inter}}$ given by the Kubo formula [26,27], with the intraband contribution σ^{intra} given by

$$\sigma^{\text{intra}}(\omega) = \frac{2ie^2T}{\pi\hbar(\omega + i\gamma_c)} \ln[2 \cosh(\mu_c/2T)], \quad (1)$$

and the interband contribution σ^{inter} given by

$$\sigma^{\text{inter}} = \frac{e^2}{4\hbar} \left\{ \Theta(\hbar\omega - 2\mu_c) - \frac{i}{\pi} \ln \left| \frac{\hbar\omega + 2\mu_c}{\hbar\omega - 2\mu_c} \right| \right\}, \quad (2)$$

where μ_c is the chemical potential (controlled with the help of a gate voltage), γ_c is the carriers scattering rate, $\Theta(x)$ is the Heaviside function, e is the electron charge, k_B is the Boltzmann constant, and \hbar is the reduced Planck constant. The intraband contribution Eq. (1) dominates for large doping $\mu_c \gg k_B T$ and is a generalization of the Drude model for the case of arbitrary band structure, whereas the interband contribution Eq. (2) dominates for large frequencies $\hbar\omega \gtrsim \mu_c$.

When the wave vector of the incident plane wave is perpendicular to the wire axis, the scattering problem can be decomposed into two independent scalar problems: electric field parallel to the main section of the cylindrical surface (p polarization, magnetic field along \hat{z}) and magnetic field parallel to the main section of the cylindrical surface (s polarization, electric field along \hat{z}). In region j ($j = 1, 2$) and for each polarization mode we denote by $\psi^{(j)}(\mathbf{r})$ the nonzero component of the total electromagnetic field along the axis of the cylinder, evaluated at the observation point $\mathbf{r} = x\hat{x} + y\hat{y}$. These field components must satisfy Helmholtz equations in each region:

$$\left(\nabla^2 + \left(\frac{\omega}{c} \right)^2 \epsilon_j \mu_j \right) \psi^{(j)} = 0, \quad j = 1, 2. \quad (3)$$

As in the case of uncoated cylinders [21–23], the starting point for the derivation of an exact expression for the scattered field is Green's second integral. Using Eq. (3) in the exterior region and separating the total field in this region into contributions from the incident and scattered field, $\psi^{(1)}(\mathbf{r}) = \psi_{\text{inc}}^{(1)}(\mathbf{r}) + \psi_{\text{sc}}^{(1)}(\mathbf{r})$, we obtain

$$\psi^{(1)}(\mathbf{r}) = \psi_{\text{inc}}^{(1)}(\mathbf{r}) + \frac{1}{4\pi} \times \int_{\Gamma} \left(\frac{\partial G^{(1)}(\mathbf{r}, \mathbf{r}')}{\partial \hat{n}'} \psi^{(1)}(\mathbf{r}') - G^{(1)}(\mathbf{r}, \mathbf{r}') \frac{\partial \psi^{(1)}(\mathbf{r}')}{\partial \hat{n}'} \right) dS', \quad (4)$$

where \mathbf{r}' is a point on the boundary Γ with arc element dS' and $G^{(1)}(\mathbf{r}, \mathbf{r}')$ is the Green function of Eq. (3) in the exterior region. Analogously, using Green's second integral and Eq. (3) in the interior region, we obtain

$$0 = \int_{\Gamma} \left(\frac{\partial G^{(2)}(\mathbf{r}, \mathbf{r}')}{\partial \hat{n}'} \psi^{(2)}(\mathbf{r}') - G^{(2)}(\mathbf{r}, \mathbf{r}') \frac{\partial \psi^{(2)}(\mathbf{r}')}{\partial \hat{n}'} \right) dS', \quad (5)$$

where $G^{(2)}(\mathbf{r}, \mathbf{r}')$ is the Green function of Eq. (3) in the interior region. Due to the cylindrical symmetry both Green functions may be expressed in terms of the zeroth-order Hankel function of the first kind $H_0^{(1)}$,

$$G^{(j)}(\mathbf{r}|\mathbf{r}') = i\pi H_0^{(1)}(k_j|\mathbf{r} - \mathbf{r}'|), \quad (6)$$

with $k_j = \frac{\omega}{c} \sqrt{\epsilon_j \mu_j}$ ($j = 1, 2$). By letting the point of observation \mathbf{r} approach the surface \mathbf{r}' in expressions Eqs. (4) and (5), we obtain a pair of integral equations with four unknown functions: the values of the fields $\psi^{(j)}$ and of their normal derivatives $\partial\psi^{(j)}/\partial\hat{n}$, $j = 1, 2$, at the boundary Γ . As in the case of uncoated cylinders, the number of unknowns can be reduced to two since the electromagnetic boundary conditions at Γ provide two additional relationships between the normal derivatives and the fields at the boundary. Taking into account that because of the graphene coating the tangential components of the magnetic field \mathbf{H} are no longer continuous across the boundary Γ —as they were in the case of uncoated cylinders—the boundary conditions for our case can be expressed as

$$\frac{1}{\epsilon_1} \frac{\partial\psi^{(1)}}{\partial\hat{n}} = \frac{1}{\epsilon_2} \frac{\partial\psi^{(2)}}{\partial\hat{n}} \quad \text{and} \quad \psi^{(1)} - \psi^{(2)} = \frac{4i\pi}{\omega\epsilon_1} \sigma \frac{\partial\psi^{(1)}}{\partial\hat{n}}, \quad (7)$$

for p polarization, and

$$\psi^{(1)} = \psi^{(2)} \quad \text{and} \quad \frac{1}{\mu_1} \frac{\partial\psi^{(1)}}{\partial\hat{n}} - \frac{1}{\mu_2} \frac{\partial\psi^{(2)}}{\partial\hat{n}} = -\frac{4i\pi\omega\sigma}{c^2} \psi^{(1)}, \quad (8)$$

for s polarization. In Eqs. (7) and (8) the fields and their normal derivatives are evaluated at $\mathbf{r} = \mathbf{r}_s(\tau)$.

The boundary conditions allow us to express $\psi^{(2)}$ and $\partial\psi^{(2)}/\partial\hat{n}$ in terms of $\psi^{(1)}$ and $\partial\psi^{(1)}/\partial\hat{n}$. Therefore, Eqs. (4) and (5) can be rewritten as a set of coupled, inhomogeneous integral equations for the unknown exterior functions $\psi^{(1)}$ and $\partial\psi^{(1)}/\partial\hat{n}$. To find these functions, the system of integral equations is converted into matrix equations, which are then solved numerically. We do this by using a set $[\tau_1, \dots, \tau_N]$ for discretizing the interval where the parameter τ describing the boundary varies. The evaluation of the matrix elements and the treatment of the Hankel functions singularities when the argument is zero follows closely that described in [21,22]. Once the functions $\psi^{(1)}$ and $\partial\psi^{(1)}/\partial\hat{n}$ are known, the scattered field, given by the second term in Eq. (4), can be calculated at every point in the exterior region. Yet another application of Green's second integral in the interior region gives the following expression for the field at every point inside the wire:

$$\psi^{(2)}(\mathbf{r}) = -\frac{i}{4} \int_{\Gamma} \left(k_2 \hat{n}' \cdot (\mathbf{r} - \mathbf{r}') \frac{H_1^{(1)}(k_2|\mathbf{r} - \mathbf{r}'|)}{|\mathbf{r} - \mathbf{r}'|} \psi^{(2)}(\mathbf{r}') - H_0^{(1)}(k_2|\mathbf{r} - \mathbf{r}'|) \frac{\partial\psi^{(2)}(\mathbf{r}')}{\partial\hat{n}'} \right) dS', \quad (9)$$

where the boundary conditions Eqs. (7) and (8) must be used to obtain the interior source functions $\psi^{(2)}$ and $\partial\psi^{(2)}/\partial\hat{n}$ in terms of the exterior source functions $\psi^{(1)}$ and $\partial\psi^{(1)}/\partial\hat{n}$.

Knowing the total electromagnetic field allows us to calculate optical characteristics, such as the scattering, absorption, and extinction cross sections [28,29]. The time-averaged total power scattered by a two-dimensional particle can be evaluated by calculating the complex Poynting vector flux through an imaginary cylinder of length L and radius r_0 that encloses the particle (see Fig. 1):

$$P_{\text{sc}} = r_0 L \int_0^{2\pi} \langle \mathbf{S}_{\text{sc}}(r_0, \theta) \rangle \cdot \hat{\mathbf{r}} d\theta, \quad (10)$$

where

$$\langle \mathbf{S}_{sc}(r_0, \theta) \rangle = \frac{c^2}{8\pi\omega\eta} \text{Re}(i\mathbf{F}(r, \theta) \times [\nabla \times \mathbf{F}(r, \theta)]^*), \quad (11)$$

and $\mathbf{F}(r, \theta) = \psi_{sc}(r, \theta)\hat{\mathbf{z}}$ and $\eta = \mu_1$ (s polarization) or $\eta = \epsilon_1$ (p polarization). Introducing Eq. (11) into Eq. (10), we obtain

$$P_{sc} = \frac{c^2 r_0 L}{8\pi\omega\eta} \int_0^{2\pi} \text{Re} \left(i\psi_{sc}(r_0, \theta) \frac{\partial \psi_{sc}^*}{\partial r} \right) d\theta. \quad (12)$$

In the far-field region the calculation of the scattered fields—given by the second term in Eq. (4)—can be greatly simplified using the asymptotic expansion of the Hankel function for large argument. After some algebraic manipulation, the following results are found:

$$\psi_{sc}(r, \theta) = -\frac{i \exp(i[k_1 r - \pi/4])}{\sqrt{8\pi k_1 r}} F_{\text{ang}}(\theta), \quad (13)$$

$$\frac{\partial \psi_{sc}^*(r, \theta)}{\partial r} = ik_1 \psi_{sc}(r, \theta), \quad (14)$$

where the angular factor $F_{\text{ang}}(\theta)$ is given by

$$F_{\text{ang}}(\theta) = \int_{J(\Gamma)} \left(ik_1 [-g'(\tau) \cos \theta + f'(\tau) \sin \theta] \psi^{(1)}(\tau) + \frac{\partial \psi^{(1)}(\tau)}{\partial \hat{n}} \exp(-ik_1 [f(\tau) \cos \theta + g(\tau) \sin \theta]) d\tau \right). \quad (15)$$

When Eqs. (13) and (14) are substituted into Eq. (12), we get

$$P_{sc} = \frac{c^2 L}{64\pi^2 \omega \eta} \int_0^{2\pi} |F_{\text{ang}}(\theta)|^2 d\theta. \quad (16)$$

The scattering efficiency Q_s is defined as the ratio between the total power scattered by the two-dimensional particle, given by Eq. (16), and the incident power P_{inc} intersected by the area DL (see Fig. 1). Analogously, the absorption efficiency Q_a is defined as the ratio between the power P_a absorbed by the graphene-wrapped two-dimensional particle and P_{inc} . P_a can be obtained as

$$P_a = -\frac{c^2 L}{8\pi\omega\eta} \int_{J(\Gamma)} \text{Re} \left(iN(\tau) \psi^{(1)}(\tau) \left[\frac{\partial \psi^{(1)}(\tau)}{\partial \hat{n}} \right]^* \right) d\tau, \quad (17)$$

with $N(\tau) = \sqrt{(f'(\tau))^2 + (g'(\tau))^2}$.

3. RESULTS AND DISCUSSION

A. Wires of Circular Section

To assess the validity of the integral formalism sketched in Section 2 for investigating light scattering and absorption in graphene-coated wires near LSP resonances, we resort to circular geometries where a reference solution exists [15–18]. In Fig. 2 we compare the numerical results obtained with the integral formalism described in this paper (solid curves) with the semi-analytical results obtained using Lorenz–Mie–Debye solution for the scattered fields in the form of infinite series of cylindrical multipole partial waves (circles). The curves in this figure represent the scattering efficiency spectra for a circular wire with a radius $R = 0.5 \mu\text{m}$, made with a nonplasmonic, transparent material ($\epsilon_2 = 3.9$, $\mu_2 = 1$) in a

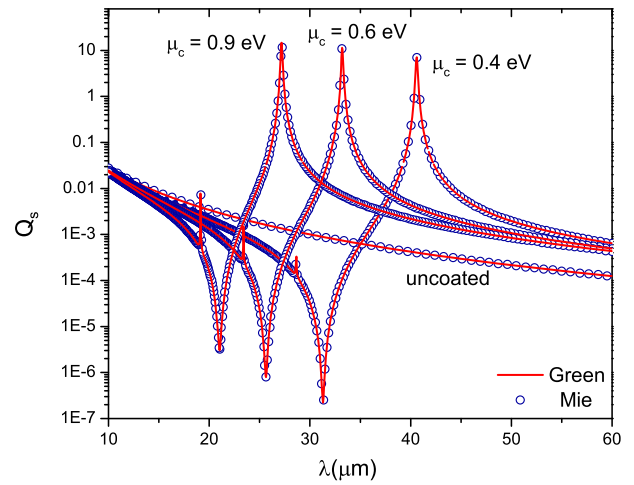


Fig. 2. Comparison between the Green and the multipolar Mie formalisms results for the p -polarized scattering efficiency Q_s of a graphene-coated circular wire with a dielectric core. $R = 0.5 \mu\text{m}$, $\epsilon_2 = 3.9$, $\mu_2 = 1$, $\mu_1 = \epsilon_1 = 1$, Kubo parameters for the graphene coating are $T = 300^\circ\text{K}$, $\gamma_c = 0.1 \text{ meV}$, and $\mu_c = 0.4, 0.6$, and 0.9 eV .

vacuum ($\mu_1 = \epsilon_1 = 1$). We used Kubo parameters $T = 300^\circ\text{K}$, $\gamma_c = 0.1 \text{ meV}$, different values of μ_c , excitation frequencies in the range between 5 THz (incident wavelength $60 \mu\text{m}$) and 30 THz (incident wavelength $10 \mu\text{m}$), and p -polarized incident waves. The curve corresponding to the uncoated wire, not showing any plasmonic feature in this spectral range, is given as a reference. An excellent agreement between both formalisms is observed in Fig. 2. The spectral position of the dipolar graphene surface plasmon resonances—at wavelengths near $40.60 \mu\text{m}$ ($\mu_c = 0.4 \text{ eV}$), $33.20 \mu\text{m}$ ($\mu_c = 0.6 \text{ eV}$), and $27.16 \mu\text{m}$ ($\mu_c = 0.9 \text{ eV}$)—also agree well with those calculated using nonretarded analytical expressions [17]. The agreement is also observed for the spectral position of the lower local maxima near $28.65 \mu\text{m}$ (for $\mu_c = 0.4 \text{ eV}$), $23.40 \mu\text{m}$ (for $\mu_c = 0.6 \text{ eV}$), and $19.13 \mu\text{m}$ (for $\mu_c = 0.9 \text{ eV}$), which correspond to quadrupolar surface current distributions in the graphene coating and are associated with a complex pole in the second coefficient of the multipole expansion (the coefficient of the term that varies twice from positive to negative around the cylinder).

To further assess the suitability of the Green formalism presented here, we repeat the comparisons for circular geometries, but with metallic (intrinsically plasmonic) cores instead of dielectric (nonplasmonic) cores. The results are shown in Fig. 3, where we show the spectral dependence of the p -polarized scattering efficiency Q_s for a graphene-coated metallic wire with $R = 50 \text{ nm}$, illuminated from vacuum. We assume that the interior electric permittivity is described by the Drude model $\epsilon_2(\omega) = \epsilon_\infty - \omega_p^2 / (\omega^2 + i\gamma_m\omega)$ with $\epsilon_\infty = 1$, $\gamma_m = 0.01 \text{ eV}$ and different values of $\hbar\omega_p$ (0.4, 0.7, and 0.9 eV). Kubo parameters for $\sigma(\omega)$ are $T = 300^\circ\text{K}$, $\gamma_c = 0.1 \text{ meV}$, and $\mu_c = 0.5 \text{ eV}$. We observe that numerical results obtained with the integral formalism (solid curves) and with the Mie solution (circles) are all again in excellent agreement. As explained in [10,16,17], the net effect of the graphene coating is to increase

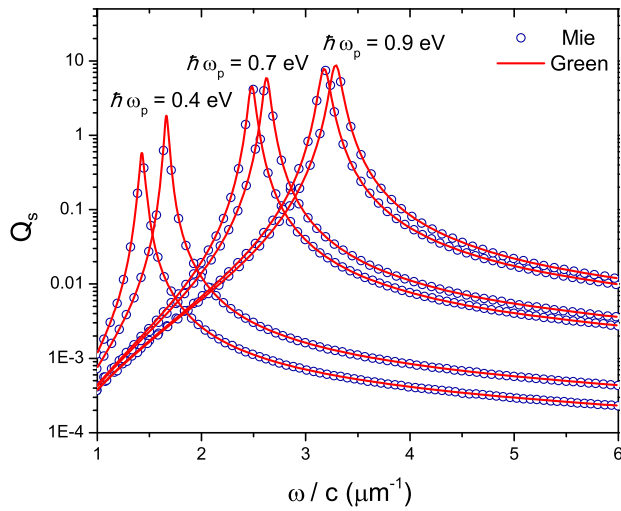


Fig. 3. Comparison between the Green and the multipolar Mie formalisms results for the p -polarized scattering efficiency Q_s of a graphene-coated circular wire with a plasmonic, metallic-like core. $R = 50$ nm, the electric permittivity of the core is described by the Drude model, $\epsilon_2(\omega) = \epsilon_\infty - \omega_p^2 / (\omega^2 + i\gamma_m\omega)$, with $\epsilon_\infty = 1$, $\gamma_m = 0.01$ eV and different values of $\hbar\omega_p$ (0.4, 0.7, and 0.9 eV), and the Kubo parameters for the graphene layer are $T = 300^\circ\text{K}$, $\gamma_c = 0.1$ meV, and $\mu_c = 0.5$ eV.

the charge density induced on the surface of the metallic particle, thus blueshifting the resonances of the metallic particle.

B. Wires of Elliptic Section

Having determined the suitability of the Green approach for the simulation of plasmon resonances in graphene-covered wires, we next explore the effects that the departure from circular geometries has on the spectrum of graphene LSPs supported by the wire. Guided by previous research on metallic nanowires with a nonregular cross section [24,25], the complexity of the resonance spectrum is expected to increase when the symmetry of the wire section decreases. In order to proceed gradually and keep some degree of control to verify the effectiveness of our Green theoretical formulation and numerical codes, we consider wires with elliptical section, a geometry which includes the circle as a special case.

In Fig. 4 we plot the scattering efficiency Q_s for p -polarized incident waves and for various angles of incidence for a graphene-coated elliptical wire with major and minor semi-axes $a = 0.55$ μm and $b = 0.45$ μm , respectively. The wire substrate is a nonplasmonic, transparent material ($\epsilon_2 = 3.9$, $\mu_2 = 1$), the medium of incidence is vacuum ($\mu_1 = \epsilon_1 = 1$), and the Kubo parameters are $T = 300^\circ\text{K}$, $\gamma_c = 0.1$ meV, and $\mu_c = 0.9$ eV. The curve corresponding to a graphene-coated wire of circular section and $a = b = 0.5$ μm is given as a reference. We observe that, similar to the case of metallic LSPs [24,25], the break of the rotational symmetry of the wire section introduces a two-dimensional anisotropy in the angular optical response. This anisotropy is particularly evident for the dipolar plasmonic resonance, which for the circular case ($a = b = 0.5$ μm) occurs near 27.16 μm and that is split into two different resonant peaks, one near 25.81 μm and the other

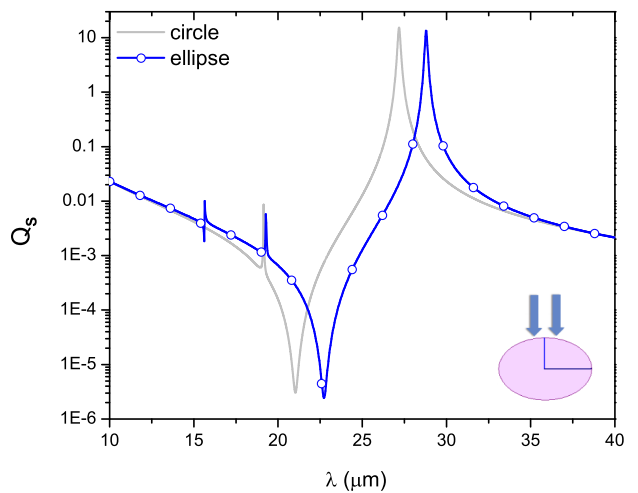
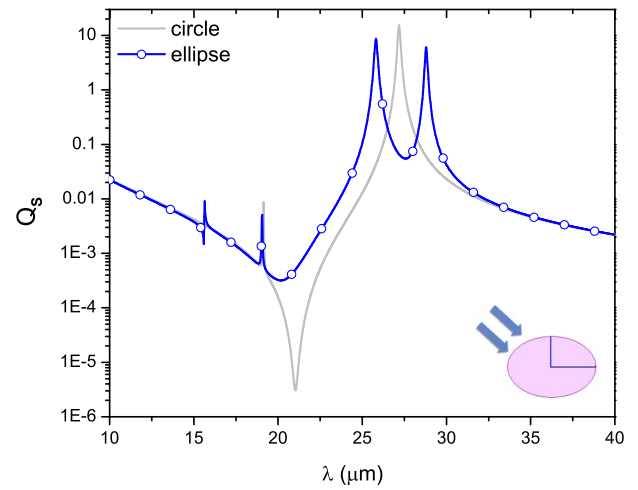
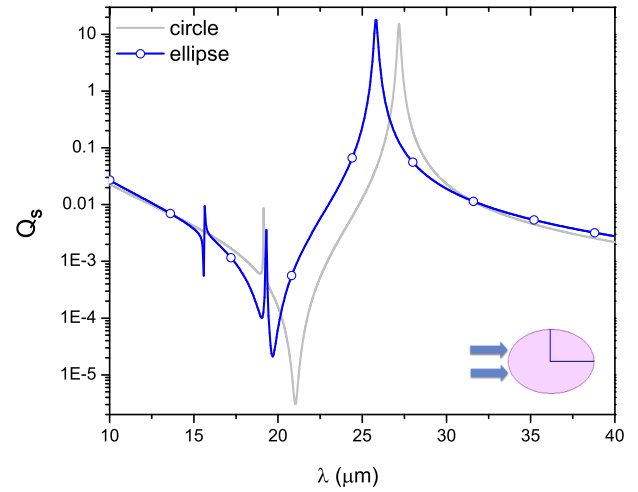


Fig. 4. Scattering efficiency Q_s for p -polarized incident waves and for illumination direction along (top), at 45° (middle), and perpendicular to (bottom) the major axis, for a graphene-coated elliptical wire with semi-axes $a = 0.55$ μm and $b = 0.45$ μm , $\epsilon_2 = 3.9$, $\mu_2 = 1$, $\mu_1 = \epsilon_1 = 1$, and Kubo parameters $T = 300^\circ\text{K}$, $\gamma_c = 0.1$ meV, and $\mu_c = 0.9$ eV. The light gray curve corresponds to a graphene-coated circular wire ($a = b = 0.5$ μm).

near $28.78 \mu\text{m}$. The first peak corresponds to the illumination direction along the ellipse's major axis while the second peak corresponds to the illumination direction perpendicular to the major axis, as clearly indicated in Fig. 4 by the fact that both resonances are decoupled for illumination directions parallel to either of the ellipse's axes and that the first (respectively second) peak is absent when the illumination direction is perpendicular to (respectively along) the major axis. We observe that while the graphene coating always introduces a minimum in the scattering efficiency of circular rods—near $21.02 \mu\text{m}$ for the parameters in Fig. 4, a relevant feature in the context of graphene invisibility cloaks [9] and corresponding to a complex zero of the first coefficient of the cylindrical multipole expansion [16]—the position and magnitude of this minimum depend strongly on the illumination direction, which is another manifestation of two-dimensional anisotropy in the angular optical response of the elliptical wire.

Although associated with weaker enhancements of the scattering efficiency, other peaks corresponding to multipolar modes higher than the dipolar mode can also be observed in Fig. 4. These higher-frequency graphene LSP modes are better appreciated in the near field, as shown in Fig. 5 where we plot absorption efficiency Q_A spectra for the same elliptical wire and directions of incidence considered in Fig. 4. The absorption spectrum corresponding to the circular case ($a = b = 0.5 \mu\text{m}$) is also given as a reference. Apart from the frequency splitting of the dipolar mode already noted in Fig. 4, we also observe a splitting in the quadrupolar resonance, which in the circular case occurs at a wavelength near $19.13 \mu\text{m}$ and that in the elliptical case is split into a peak near $19.27 \mu\text{m}$, corresponding to illumination directions parallel to the ellipse's axes, and another peak near $19.06 \mu\text{m}$, the only resolved peak when the illumination direction makes an angle of 45° with the ellipse's axes.

In agreement with the results shown in Fig. 3 for graphene-coated metallic rods of circular section, in the elliptical case the

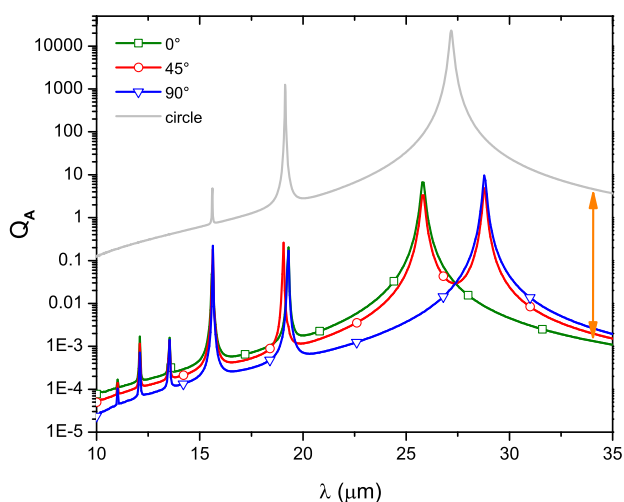


Fig. 5. Absorption efficiency for different angles of incidence for the same elliptical wire considered in Fig. 4. The illumination direction (i) is along the ellipse's major axis (0°); (ii) makes an angle of 45° with the ellipse's axes; and (iii) is perpendicular to the ellipse's major axis (90°). The light gray curve corresponds to a graphene-coated circular wire and is displaced, for clarity, by the magnitude indicated by the double-headed arrow.

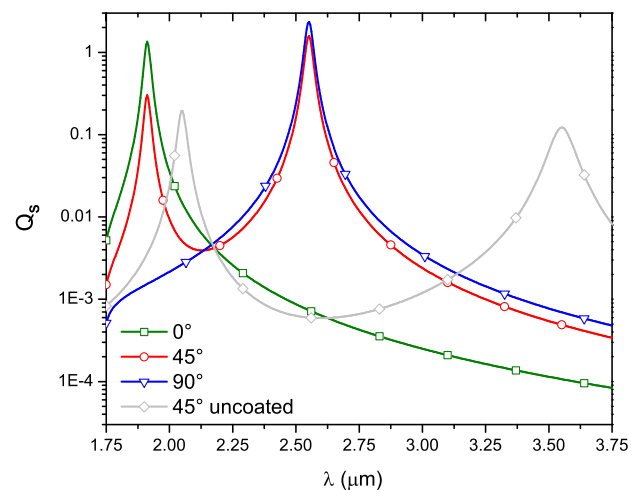


Fig. 6. Scattering efficiency spectra for a graphene-coated elliptical wire ($a = 0.03 \mu\text{m}$ and $b = 0.01 \mu\text{m}$) with a plasmonic, metallic core. The electric permittivity of the core is described by the Drude model, $\epsilon_2(\omega) = \epsilon_\infty - \omega_p^2/(\omega^2 + i\gamma_m\omega)$, with $\epsilon_\infty = 1$, $\gamma_m = 0.01 \text{ eV}$, and $\hbar\omega_p = 0.7 \text{ eV}$. The Kubo parameters for the graphene layer are $T = 300\text{K}$, $\gamma_c = 0.1 \text{ meV}$, and $\mu_c = 0.7 \text{ eV}$. The illumination direction (i) is along the ellipse's major axis (0°); (ii) makes an angle of 45° with the ellipse's axes; and (iii) is perpendicular to the ellipse's major axis (90°). The curve corresponding to the bare elliptical wire illuminated at an angle of 45° with the ellipse's axes is given as a reference.

enhancements of the scattering efficiency are significant only for the dipolar mode. This is shown in Fig. 6, where we observe that the dipolar resonance is now split into two peaks corresponding to illumination directions perpendicular and parallel to the ellipse's major axis. The curve corresponding to the bare elliptical wire illuminated at an angle of 45° with the ellipse's axes is given as a reference. We note that both dipolar resonances are blueshifted compared to those of the bare wire, in complete agreement with the fact that the net effect of the graphene coating is to increase the induced charge density on the cylindrical surface of the metallic wire [16,17]. Graphene-coated plasmonic particles are particularly attractive because their scattering and absorption characteristics can be tuned by varying the graphene chemical potential μ_g with the help of a constant electric field (electric field effect, gate voltage), and not only by changing their size or their dielectric constant, as is the case for metallic particles. To illustrate this tunability for elliptical wires, we show in Fig. 7 the scattering efficiency Q_s for the wire considered in Fig. 5 and three different values of the chemical potential, $\mu_c = 0.5 \text{ eV}$, 0.7 eV , and 1.0 eV . The illumination direction makes an angle of 45° with the major axis of the ellipse and the incident wave is p -polarized. We observe that the value of the chemical potential influences the position of the multipolar resonances and the magnitude of the splitting. In Fig. 8 we plot the spatial distribution of the field normalized to the incident amplitude for the wire considered in Figs. 4 and 5. In Fig. 8(a) the incident wavelength is $\lambda = 25.81 \mu\text{m}$ and the illumination direction is along the ellipse's major axis (0°) whereas in Fig. 8(b) the incident wavelength is $\lambda = 28.78 \mu\text{m}$ and the illumination direction is along the ellipse's minor axis (90°). We observe that in both cases the wire is behaving as an

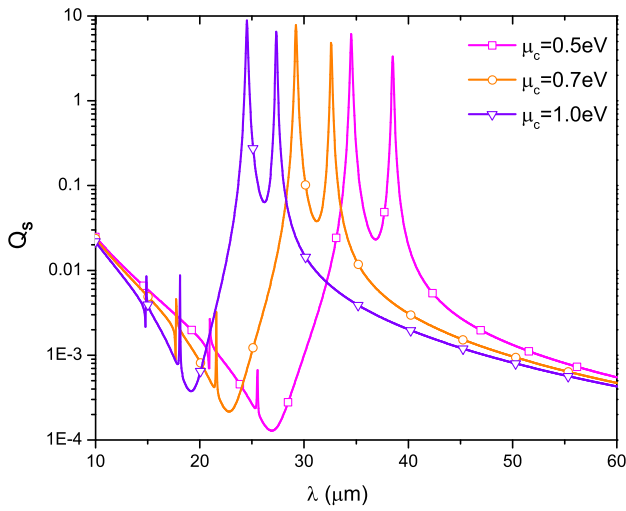


Fig. 7. Scattering efficiency Q_s for an elliptical wire with three different values of the chemical potential μ_c . The illumination direction makes an angle of 45° with the major axis of the ellipse; the other constitutive and geometrical parameters are the same as those considered in Fig. 5.

oscillating electric dipole oriented along the direction of the incident field, that is, along the ellipse’s minor axis in Fig. 8(a) or along the ellipse’s major axis in Fig. 8(b). Figure 8(c), corresponding to an incident wavelength $\lambda = 25.81 \mu\text{m}$ and illumination direction making an angle of 45° with the ellipse’s axes, shows that in these conditions the electric field inside the wire is parallel to the minor axis, although the components of the incident field along both ellipse’s axes have equal magnitude. Figure 8(d), corresponding to the incident wavelength

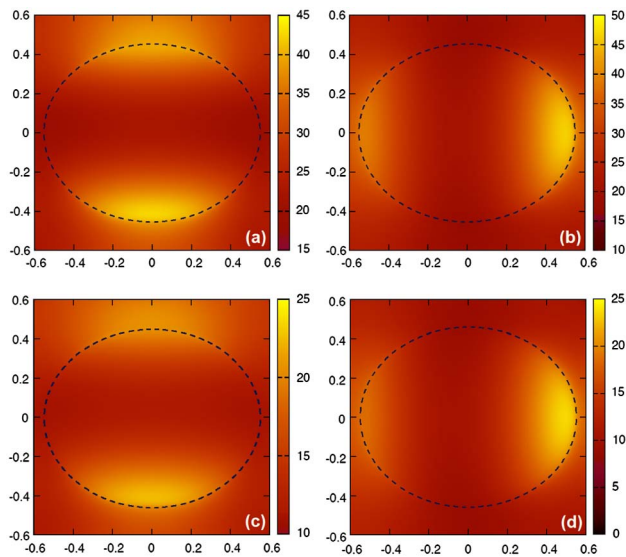


Fig. 8. Map of the near field $|\vec{H}(x,y)|$ for the graphene-coated elliptical cylinder considered in Figs. 4 and 5. (a) $\lambda = 25.81 \mu\text{m}$, illumination direction along the ellipse’s major axis (0°); (b) $\lambda = 28.78 \mu\text{m}$, illumination direction along the ellipse’s minor axis (90°); (c) $\lambda = 25.81 \mu\text{m}$, illumination direction at 45° with the ellipse’s axes; (d) $\lambda = 28.78 \mu\text{m}$, illumination direction at 45° with the ellipse’s axes.

$\lambda = 28.78 \mu\text{m}$ and illumination direction at 45° with the ellipse’s axes, shows a similar behavior, except that now the electric field inside the wire is parallel to the major axis, despite the fact that the components of the incident field along both ellipse’s axes have equal magnitude. The results in Figs. 8(c) and 8(d) are a clear confirmation that the values $\lambda = 25.81 \mu\text{m}$ and $\lambda = 28.78 \mu\text{m}$ correspond to the splitting of the degenerate dipolar resonance of the circular wire, as suggested in Figs. 4 and 5 by the correspondence between the scattering and absorption efficiency spectra for low-eccentricity elliptical and circular wires.

The agreement between the multipolar order revealed by the topology of the near field on the one hand and that suggested by the correspondence between spectra for circular and for low-eccentricity elliptical wires on the other hand is also observed for higher-frequency peaks. This is illustrated by the panel in Fig. 9, showing near-field maps for three illumination directions: at 45° with the ellipse’s axes (top row), along the ellipse’s minor axis (middle row), and along the ellipse’s major axis (bottom row). The near-field maps in the left column correspond to the quadrupolar resonance, in the circular case ($a = b = 0.5 \mu\text{m}$) located near $19.13 \mu\text{m}$ and split into two

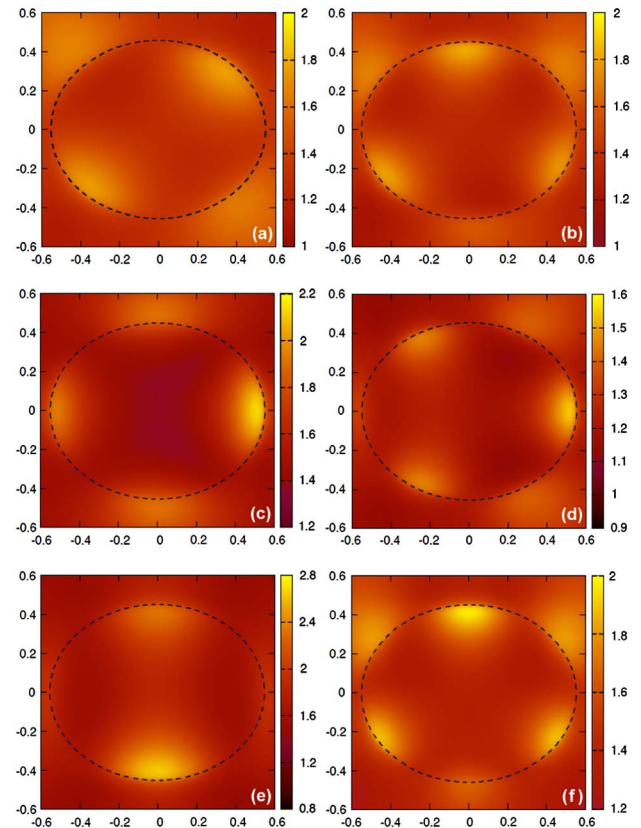


Fig. 9. Map of the near field $|\vec{H}(x,y)|$ for the graphene-coated elliptical cylinder considered in Figs. 4 and 5. (a) $\lambda = 19.06 \mu\text{m}$, illumination direction at 45° with the ellipse’s axes; (b) $\lambda = 15.64 \mu\text{m}$, illumination direction at 45° with the ellipse’s axes; (c) $\lambda = 19.27 \mu\text{m}$, illumination direction along the ellipse’s minor axis (90°); (d) $\lambda = 15.64 \mu\text{m}$, illumination direction along the ellipse’s minor axis (90°); (e) $\lambda = 19.27 \mu\text{m}$, illumination direction along the ellipse’s major axis (0°); (f) $\lambda = 15.64 \mu\text{m}$, illumination direction along the ellipse’s major axis (0°).

close resonant peaks, one at $\lambda = 19.27 \mu\text{m}$, associated with field enhancements near vertices and co-vertices, and the other at $\lambda = 19.06 \mu\text{m}$, associated with field enhancements near the diagonals of the rectangle circumscribed to the ellipse. The maps in the right column correspond to hexapolar resonances near $\lambda = 15.64 \mu\text{m}$ (near $15.61 \mu\text{m}$ in the circular case). Although the topology of the hexapolar near field when the illumination direction is at 45° with the ellipse's axes is very different to the topology when the illumination direction is along the axes, symmetry-breaking splittings of the hexapolar peaks are not resolvable in the scattering and absorption efficiency spectra.

4. SUMMARY AND CONCLUSIONS

In conclusion, we have presented in this paper an electromagnetically rigorous method based on Green's second identity for studying the plasmonic response of graphene-coated wires of arbitrary shape. To validate the method, we compare the numerically computed scattering and absorption efficiencies in the particular case of graphene-coated wires of circular section with the results obtained from a multipolar Mie theory. All the results agree excellently, for both metallic and dielectric substrates. To explore the effects that the break of the rotational symmetry of the wire section has in the plasmonic features of the scattering and absorption response, we apply the Green formulation to the case of graphene-coated wires of elliptical section. Compared with the scattering and absorption efficiency spectra for graphene-coated wires of circular section, and as it might be expected on symmetry grounds, a frequency splitting of multipolar plasmonic resonances is observed in the spectra for low-eccentricity elliptical wires. To illustrate the application of the Green method in the near field we investigate the spatial distribution of the electromagnetic field near the graphene coating for different frequencies and directions of incidence. As a further test on the validity of the Green formulation, we show that the multipolar order revealed by the topology of the near field agrees perfectly well with the multipolar order obtained from the correspondence between spectra for circular and for low-eccentricity elliptical wires. The method presented here should be useful in the design and engineering of graphene-wrapped particles with tailored properties for specific plasmonic applications, including photovoltaic devices, nanoantennas, switching, biosensing, and even medical treatments.

Funding. Consejo Nacional de Investigaciones Científicas y Técnicas (CONICET) (PIP 1800); Universidad de Buenos Aires (UBA) (UBA 20020100100327); Universidad Autónoma de Baja California (AUBC); Consejo Nacional de Ciencia y Tecnología (CONACYT).

REFERENCES

1. A. K. Geim, "Graphene: status and prospects," *Science* **324**, 1530–1534 (2009).
2. F. Bonaccorso, L. Colombo, G. Yu, M. Stoller, V. Tozzini, A. Ferrari, R. Ruoff, and V. Pellegrini, "Graphene, related two-dimensional crystals, and hybrid systems for energy conversion and storage," *Science* **347**, 1246501 (2015).
3. A. C. Ferrari, F. Bonaccorso, V. Falco, K. S. Novoselov, S. Roche, P. Bøggild, S. Borini, F. H. L. Koppens, V. Palermo, N. Pugno, J. A. Garrido, R. Sordan, A. Bianco, L. Ballerini, M. Prato, E. Lidorikis, J. Kivioja, C. Marinelli, T. Ryhänen, A. Morpurgo, J. N. Coleman, V. Nicolosi, L. Colombo, A. Fert, M. Garcia-Hernandez, A. Bachtold, G. F. Schneider, F. Guinea, C. Dekker, M. Barbone, Z. Sun, C. Galiotis, A. N. Grigorenko, G. Konstantatos, A. Kis, M. Katsnelson, L. Vandersypen, A. Loiseau, V. Morandi, D. Neumaier, E. Treossi, V. Pellegrini, M. Polini, A. Tredicucci, G. M. Williams, B. H. Hong, J.-H. Ahn, J. M. Kim, H. Zirath, B. J. van Wees, H. van der Zant, L. Occhipinti, A. Di Matteo, I. A. Kinloch, T. Seyller, E. Quesnel, X. Feng, K. Teo, N. Rupesinghe, P. Hakonen, S. R. Neil, Q. Tannock, T. Löfwander, and J. Kinaret, "Science and technology roadmap for graphene, related two-dimensional crystals, and hybrid systems," *Nanoscale* **7**, 4598–4810 (2015).
4. F. M. Kin, J. Long, W. Feng, and T. F. Heinz, "Optical spectroscopy of graphene: from the far infrared to the ultraviolet," *Solid State Commun.* **152**, 1341–1349 (2012).
5. M. Grande, T. Stomeo, G. V. Bianco, M. A. Vincenti, D. de Ceglia, V. Petruzzelli, G. Bruno, M. De Vittorio, M. Scalora, and A. D'Orazio, "Fabrication of doubly resonant plasmonic nanopatch arrays on graphene," *Appl. Phys. Lett.* **102**, 231111 (2013).
6. M. Hashemi, M. H. Farzad, N. A. Mortensen, and S. Xiao, "Enhanced absorption of graphene in the visible region by use of plasmonic nanostructures," *J. Opt.* **15**, 055003 (2013).
7. M. Jablan, M. Soljacic, and H. Buljan, "Plasmons in graphene: fundamental properties and potential applications," *Proc. IEEE* **101**, 1689–1704 (2013).
8. T. Low and P. Avouris, "Graphene plasmonics for terahertz to mid-infrared applications," *ACS Nano* **8**, 1086–1101 (2014).
9. M. Farhat, C. Rockstuhl, and H. Bagci, "A 3D tunable and multi-frequency graphene plasmonic cloak," *Opt. Express* **21**, 12592–12603 (2013).
10. T. Christensen, A. P. Jauho, M. Wubs, and N. Mortensen, "Localized plasmons in graphene-coated nanospheres," *Phys. Rev. B* **91**, 125414 (2015).
11. B. Yang, T. Wu, Y. Yang, and X. Zhang, "Tunable subwavelength strong absorption by graphene wrapped dielectric particles," *J. Opt.* **17**, 035002 (2015).
12. Z.-R. Huang, L.-L. Wang, B. Sun, M.-D. He, J.-Q. Liu, H.-J. Li, and X. Zhai, "A mid-infrared fast-tunable graphene ring resonator based on guided-plasmonic wave resonance on a curved graphene surface," *J. Opt.* **16**, 105004 (2014).
13. T. J. Arruda, A. S. Martinez, and F. A. Pinheiro, "Electromagnetic energy within coated cylinders at oblique incidence and applications to graphene coatings," *J. Opt. Soc. Am. A* **31**, 1811–1819 (2014).
14. J. Zhao, X. Liu, W. Qiu, Y. Ma, Y. Huang, J.-X. Wang, K. Qiang, and J.-Q. Pan, "Surface-plasmon-polariton whispering-gallery mode analysis of the graphene monolayer coated InGaAs nanowire cavity," *Opt. Express* **22**, 5754–5761 (2014).
15. R. J. Li, X. Lin, S. S. Lin, X. Liu, and H. S. Chen, "Tunable deep-subwavelength superscattering using graphene monolayers," *Opt. Lett.* **40**, 1651–1654 (2015).
16. M. Riso, M. Cuevas, and R. A. Depine, "Tunable plasmonic enhancement of light scattering and absorption in graphene-coated subwavelength wires," *J. Opt.* **17**, 075001 (2015).
17. M. Cuevas, M. Riso, and R. A. Depine, "Complex frequencies and field distributions of localized surface plasmon modes in graphene-coated subwavelength wires," *J. Quant. Spectrosc. Radiat. Transfer* **173**, 26–33 (2015).
18. E. Velichko, "Evaluation of a graphene-covered dielectric microtube as a refractive-index sensor in the terahertz range," *J. Opt.* **18**, 035008 (2016).
19. N. Kumar and S. Kumbhat, *Essentials in Nanoscience and Nanotechnology* (Wiley, 2016).
20. L. Ju, B. Geng, J. Horng, C. Girit, M. Martin, Z. Hao, H. A. Bechtel, X. Liang, A. Zettl, Y. R. Shen, and F. Wang, "Graphene plasmonics for tunable terahertz metamaterials," *Nat. Nanotechnol.* **6**, 630–634 (2011).
21. A. A. Maradudin, T. Michel, A. McGurn, and E. R. Mendez, "Enhanced backscattering of light from a random grating," *Ann. Phys.* **203**, 255–307 (1990).
22. C. Valencia, E. Méndez, and B. Mendoza, "Second harmonic generation in the scattering of light by two-dimensional particles," *J. Opt. Soc. Am. B* **20**, 2150–2161 (2003).

23. W. Yan, N. Mortensen, and M. Wubs, "Green's function surface-integral method for nonlocal response of plasmonic nanowires in arbitrary dielectric environments," *Phys. Rev. B* **88**, 155414 (2013).
24. J. P. Kottmann, O. J. F. Martin, D. R. Smith, and S. Schultz, "Plasmon resonances of silver nanowires with a nonregular cross section," *Phys. Rev. B* **64**, 235402 (2001).
25. J. P. Kottmann, O. J. F. Martin, D. R. Smith, and S. Schultz, "Field polarization and polarization charge distributions in plasmon resonant nanoparticles," *New J. Phys.* **2**, 27 (2000).
26. S. A. Mikhailov and K. Sieglar, "New electromagnetic mode in graphene," *Phys. Rev. Lett.* **99**, 016803 (2007).
27. L. A. Falkovsky, "Optical properties of graphene and IV-VI semiconductors," *Phys. Usp.* **51**, 887–897 (2008).
28. M. Mishchenko, L. D. Travis, and A. A. Lacis, *Scattering, Absorption, and Emission of Light by Small Particles* (Cambridge University, 2002).
29. C. F. Bohren and D. R. Huffman, *Absorption and Scattering of Light by Small Particles* (Wiley, 1983).